

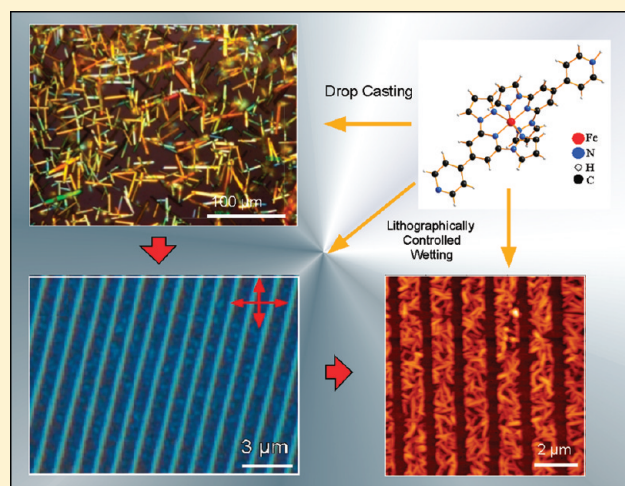
Thin Deposits and Patterning of Room-Temperature-Switchable One-Dimensional Spin-Crossover Compounds

Massimiliano Cavallini,^{*,†} Ilaria Bergenti,[†] Silvia Milita,[‡] Jean Crispin Kengne,[†] Denis Gentili,[†] Giampiero Ruani,[†] Ivan Salitros,[§] Velimir Meded,[§] and Mario Ruben[§]

[†]Institute for Nanostructured Materials (ISMN) and [‡]Institute for Microelectronic and Microsystems (IMM), CNR, Bologna, Italy

[§]Institute of Nanotechnology, Forschungszentrum Karlsruhe, Germany

ABSTRACT: We present a study on thin deposits and patterning of 1-D spin-crossover compounds $\text{Fe}^{\text{II}}\text{-(L)}_2\text{H}(\text{ClO}_4)_3 \cdot \text{MeOH}$ [$\text{L} = 4'-(4''\text{-pyridyl})-1,2':6'1''\text{-bis-(pyrazolyl)pyridine}$] (**1**) that exhibit a reversible, thermally driven spin transition at room temperature. Micrometric rodlike crystals of **1** on silicon surfaces are achieved by drop casting and solvent annealing. We observed that the crystallinity of thin deposits and spin-transition properties critically depends on the deposition procedure. Furthermore, we proved processability and patterning using unconventional wet lithography that reduces the crystallite formation time by 1 order of magnitude. Thin deposits of **1** were characterized by atomic force microscopy, polarized optical microscopy and X-rays, and the switching properties were characterized by Raman spectroscopy.



INTRODUCTION

Spin-transition compounds, also named spin-crossover (SCO) compounds, are multifunctional switching materials proposed for several technological application in molecular memories, sensors, and displays.^{1–7}

Particular interest was attracted by the SCO of Fe(II) metal ions in an octahedral ligand field because by populating the respective t_{2g} and e_g d-orbital sets their $3d^6$ valence shell may exist in its diamagnetic ($S = 0$) low-spin (LS) state as well as in its paramagnetic ($S = 2$) high-spin (HS) state.

The switching process is due to the change in splitting of the d level of the transition metal that induces the electron redistribution in d levels. The spin transition is triggered by external stimuli such as temperature, pressure, and electromagnetic radiation, and it is associated with the switching of other functional properties such as the color, conductivity, and dielectric constant.^{2,8–13}

One of the most important classes of these material includes the 1-D SCO of Fe metal ions because of their bistability features and the tendency to show high degrees of cooperativity in the solid state. Furthermore, they offer large variability in the chemical structure and composition.¹⁴

A key parameter in the use of these materials in real devices is the transition temperature; in this respect, much effort has been expended to synthesize materials with transition temperatures close to room temperature, an abrupt spin change, the presence of a wide thermal hysteresis loop, and compound stability.^{4,5}

Several SCO compounds with a room-temperature or above-room-temperature transition have been proposed in the past decade.^{15–17} Among them, materials suitable for surface deposition,¹⁸ nanocrystals,¹⁹ and nanoparticles^{19–21} have attracted particular attention with respect to possible application.

SCO properties are very fragile and critically depend on the molecular environment (e.g., packing, crystallinity, solvent molecules, anions, etc.)²² and processing, thus a great amount of effort has been expended toward the development of procedures that are able to fabricate thin deposits, films, and patterned nanostructures that preserve their switching properties. It is known that although the SCO phenomenon was first discovered more than 70 years ago^{23,24} only recently has a breakthrough toward applications been reported with the fabrication of thin films^{25–28} and ordered patterning, which allows us to address single nanostructures. In view of this fragility, the patterning of microcrystalline thin deposits is a possible way to preserve the SCO switching properties and thus drive them toward technological application.

SCO patterning has been carried out by using electron beam lithography,^{29,30} polymeric masks,³¹ and soft and unconventional lithography.^{6,32,33} In recent work,⁶ our group proved that unconventional and soft lithography can be used to fabricate reliably

Received: December 9, 2010

Revised: January 18, 2011

Published: March 02, 2011

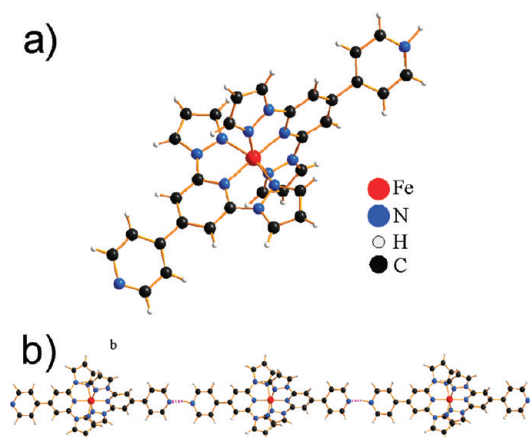


Figure 1. (a) Crystal structure of $\text{Fe}^{\text{II}}\text{-(L)}_2\text{H}](\text{ClO}_4)_3 \cdot \text{MeOH}$ [$\text{L} = 4' \text{-(4''''-pyridyl)-1,2':6'1''-bis-(pyrazolyl) pyridine}$] (**1**). (b) Supramolecular hydrogen-bonded linkage of complex cation $[\text{Fe}(\text{L}_2\text{H})]^{3+}$ of **1**.

addressable nanopatterns of SCO compounds while preserving the switching properties. In this pioneering prototype work, *cis*-bis(thiocyanato)-bis(1,10-phenanthroline)- Fe^{II} SCO compounds that exhibit an LS \leftrightarrow HS transition at 176 K was used. More recently, Thibault et al. reported on micropatterns of SCO nanoparticles by microtransfer molding.³⁴

Here we report a study of thin deposits and the patterning of a room-temperature-switchable 1-D spin-crossover compound, which further contributes to SCO application.

Because the information created in a spin-transition switching event occurs within the nanometric regime, the interfacing of the molecular switching units with the microscaled device environment is of crucial importance. Furthermore, because SCOs are paramagnetic materials, an ordered pattern of molecular aggregates is technologically more relevant than individually isolated molecules dispersed on a surface in view of developing new storage media.¹

Here we used 1-D SCO complex **1** with molecular formula $\text{Fe}^{\text{II}}\text{-(L)}_2\text{H}](\text{ClO}_4)_3 \cdot \text{MeOH}$ [$\text{L} = 4' \text{-(4''''-pyridyl)-1,2':6'1''-bis-(pyrazolyl) pyridine}$] (**1**) whose structure is shown in Figure 1a. Complex **1** is a known material that crystallizes to form an infinite 1-D chain exhibiting a spin transition at 286 K³⁵ (Figure 1b).

A major effort in nanotechnology has been devoted to the patterning of active materials into addressable size- and shape-controlled structures because of the ambitious goal of controlling physical properties through the control of material length scales. For this purpose, **1** was processed via unconventional wet lithography.^{33,36}

The use of unconventional lithography is particularly interesting because in confined systems characteristic time scales for self-organization change with the volume and dimensionality.³⁷ Quasi-equilibrium conditions can be attained on shorter time-scales, provided that the physical dimension of the system is reduced in size.³⁸ This may imply, for instance, an enhancement of surface nucleation effects and the disappearance of diffusion-limited processes.

With the aim of controlling the spatial distribution and the morphology of thin deposits, we have used lithographically controlled wetting (LCW),^{38,39} which is a technique similar to microfluidics⁴⁰ that is used to pattern materials such as molecular magnets,⁴¹ fluorescent molecules,⁴² organic semiconductors,³⁷ biomolecules,^{43,44} and magnetic precursors.⁴⁵ Here, LCW was

applied to pattern micrometric and submicrometric structures of **1** on silicon surfaces.

EXPERIMENTAL SECTION

Materials. Thin deposits of **1** were prepared by drop casting 20 μL of a 1 g/L solution in *N,N*-dimethylformamide on silicon. The substrates consist of a $10 \times 10 \text{ mm}^2$ piece of silicon covered with 200 nm of thermal oxides. It was cleaned by sonication for 2 min in electronic-grade water (Milli-Q-pure quality), 2 min in acetone (Aldrich chromatography quality), and then 2 min in 2-propanol (Aldrich spectroscopic-grade quality). The solutions were prepared using *N,N*-dimethylformamide (Aldrich, $\geq 99\%$ purity).

Stamps for Lithography. Elastomeric poly(dimethylsiloxane) (Sylgard 184 Down Corning) stamps were prepared by replica molding a blank or nonblank compact disk support that acts as a structured master. The curing process was carried out for 6 h at 60 °C. Once cured, the replica was peeled off of the master and washed in pure ethanol for 1 h. The stamp motif consists of parallel lines with a periodicity of 1.5 μm , a width at half height of 1 μm , and a depth of 200 nm.

Atomic Force Microscopy. AFM images were recorded with a commercial AFM (NT-MDT Smena) operated in air in semicontact mode (relative humidity 55%). Single-crystal silicon (N-type, 0.01–0.025 $\Omega\text{-cm}$), antimony-doped NSG10 cantilevers with a typical tip curvature radius of 10 nm were used. All images are unfiltered; only a line-by-line background subtraction has been performed to remove trend effects by NT-MDT images treatment software.

Raman. Raman scattering measurements were recorded in back-scattering geometry using a 50 \times objective at a 632.8 nm excitation wavelength with laser power in the range of 10–20 μW . The temperature range was achieved by a Peltier cooling stage in a controlled nitrogen atmosphere mounted on a micro *xyz* stage.

Optical Microscopy. Optical micrographs were recorded with a Nikon i-80 microscope equipped with an epi-illuminator and dark-field and crossed polarizers using a 100 \times objective.

X-ray Diffraction. Specular XRD measurements ($2\theta/\omega$ scan) have been carried out with a diffractometer equipped with a rotating anode source (model SmartLab of Rigaku Company). A focus line X-ray beam (Cu $K\alpha$) was collimated by a parabolic graded multilayer mirror placed in front of the sample, and a double slit was mounted in front of the detector to achieve the required angular resolution. GID-2D images have been collected at the XRD1 beamline at ELETTRA (Trieste, Italy) by using a monochromatic beam of 1.5498 Å. The incident angle was about 1°, and the 2D CCD camera was placed normal to the incident beam direction at 138 mm to record the diffraction pattern.

RESULTS AND DISCUSSION

The samples were investigated by atomic force microscopy (AFM), polarized optical microscopy, X-ray diffraction (XRD), and Raman spectroscopy.

The nature of the deposited materials strongly depends on the experimental conditions. In particular, we have observed a critical dependence on the shrinkage rate of the solvent. The change in the shrinkage is achieved by changing the partial pressure of the solvent. In particular, we compared samples obtained by drop casting in air (shrinkage time ~ 30 min) with samples prepared by drop casting in a quasi-saturated solvent atmosphere (shrinkage time ~ 24 h). The quasi-saturated atmosphere was obtained by inserting a backer with pure solvent in the box containing the drop-cast material. A small aperture in the box permits slow solvent evaporation under the quasi-equilibrium condition.⁴⁶

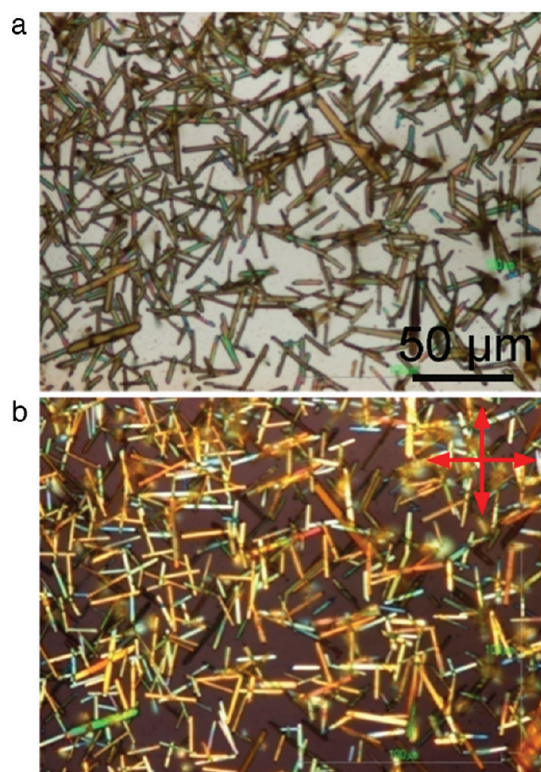


Figure 2. (a) Optical bright-field micrograph of a thin deposit of **1**. (b) Corresponding image with cross polarizers.

To reach the equilibrium condition, the backer with pure solvent is inserted inside the box more than 1 h before the sample is inserted. All of the experiments were performed at room temperature.

Figure 2 shows thin deposits of **1** after solvent annealing; thin deposits exhibit rodlike crystals randomly distributed on the surface. According to effects observed in the case of the shrinkage of a droplet with a pinned solution,⁴⁷ a higher quantity of crystals are observed at the boundary of the drop. We have estimated from the optical micrographs that the number of crystals present at the boundary is about 3 times higher than at the center of the drop. The crystal length ranges from 5 to 50 μm with an aspect ratio (length-to-width ratio) of $1:10 \pm 1.2$.

The observation under the crossed-polarizer condition (Figure 2b) shows the typical behavior of optically anisotropic materials^{46,48} (i.e., the crystals appear to be colored, where the colors, which range from green to yellow, depend on the crystal thickness).

More than 90% of the crystals appear to be homogeneously colored, which indicates that their thickness is almost constant over the entire crystal but can change for different crystals. Moreover, by rotating the microscope stage (viz., the crystal orientation vs the polarized light), the crystals are extinguished (become dark) in four positions at intervals of 90° . The occurrence of light extinction for each complete crystal at the same orientation suggests that the crystalline domains were grown in the same direction.

However, samples grown in the high shrinkage regime appear to be inhomogeneous and no clear birefringence was observed. The different appearance of the samples deposited in the slow shrinkage regime, compared to those for samples obtained in high shrinkage regime and the losses of transition properties (see also Raman characterization), is consistent with the fact that this class

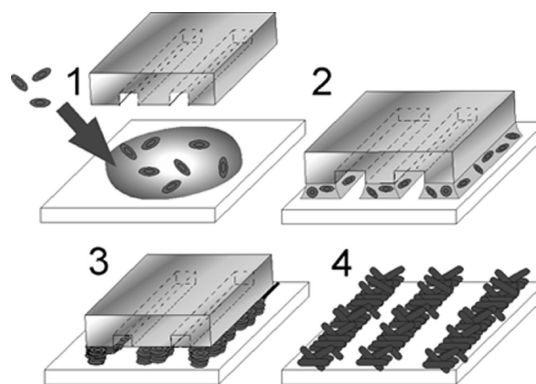


Figure 3. Scheme of lithographically controlled wetting (LCW).

of compounds is fragile to manipulate and needs to be processed in a well-controlled way.

Patterning. Compound **1** was patterned by LCW. Here a stamp made of poly(dimethylsiloxane) whose motif consists of parallel protruding lines (200 nm thickness, 1.0 μm width, and 1.5 μm pitch) is placed in contact with a liquid film of a solution of **1**, spread on a substrate. The menisci form under the stamp protrusions because of the onset of capillary forces. As the solvent evaporates, the solution remains pinned to the protrusions and the contact line between solution and substrate recedes because of faster solvent evaporation in the region between protrusions. This makes the region between the protrusions free of solution. As the critical concentration is reached, the solute precipitates onto the substrate only below the protrusions, giving rise to a structured thin film that replicates the positive pattern on the stamp. A scheme of the process is shown in Figure 3.

The self-organization of **1** starts to play a role in the later stages of shrinkage, in particular when the solution reaches supersaturation. Under such conditions, **1** starts to crystallize into micrometric crystals.

Optical and AFM studies of the printed structures reveal the formation of striplike structures of 1 μm width (Figure 4) according to the size of the stamp.

The optical image performed by polarized optical microscopy (Figure 4a) shows a slight birefringence without complete extinction at any orientation. The evidence of light extinction only in small and well-defined regions of the stripes indicates that several domains, whose length ranges from 1 to 2 μm , form each stripe. The stripes appear to be homogeneously colored; this indicates that their thickness is almost constant over the entire patterned zone.

A detailed analysis of the morphology by AFM (Figure 4b) shows that each stripe is formed by rodlike crystallites. No material in between the stripes was observed by AFM. Noticeably, while using drop-casting crystals formed in >24 h, by using LCW crystals spontaneously form within 1 h. No evidence of preferential orientation was observed inside each stripe by AFM or XRD.

The switchability of thin deposits and patterns of **1** was investigated by microRaman spectroscopy, and this has been recognized to be an efficient method for detecting the spin state in SCO compounds.⁴⁹ Furthermore, under our conditions the small laser spot size ($<1.5 \mu\text{m}$) allows the detection of the spin state with the resolution of a single crystallite.

The He–Ne excitation wavelength (632.8 nm) was used to obtain Raman spectra in the 100–2600 cm^{-1} range. Raman scattering measurements were recorded in backscattering

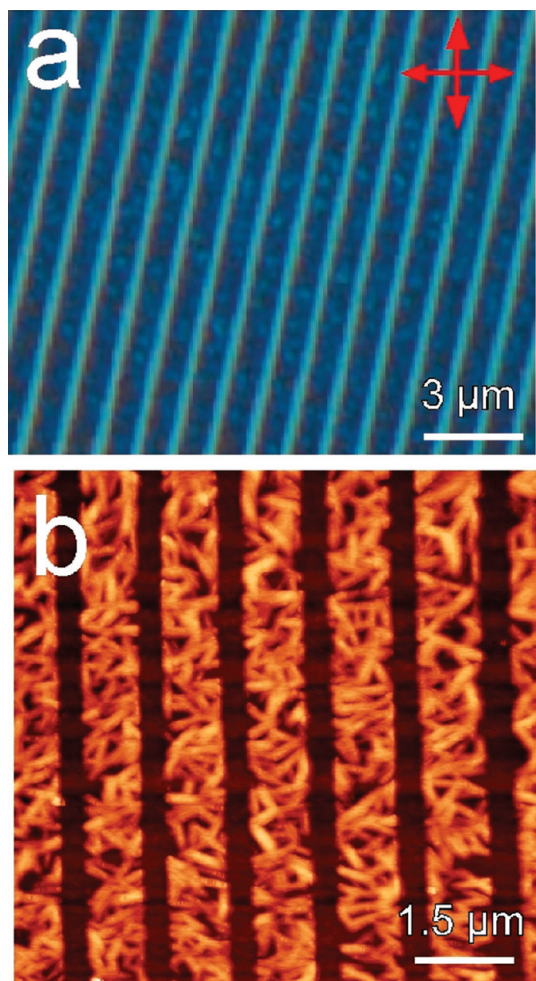


Figure 4. (a) Optical micrograph of printed microstripes of **1**. (b) Corresponding AFM morphology (z scale = 0–70 nm).

configuration using a long-working-distance $50\times$ microscope objective with laser power in the range of 10–20 μW . The samples were mounted in a liquid nitrogen Peltier heating–cooling stage to span the 150–400 K temperature range. Recycled nitrogen gas was used to purge the microscope stage of moisture and prevent condensation. To obtain good thermalization, samples were glued to the stage of the cryostat using a thermally conductive paste and slow cooling/heating rates (1 K/min) were adopted.

According to magnetic characterization, Raman spectra performed on powders and thin deposits were collected at 170 K corresponding to the complete transformation of the thin deposit in the LS state and at 393 K corresponding to the complete transformation of the thin deposit in the HS state in accordance with the magnetic measurement performed on the powder.³⁵ Figure 5a shows the Raman spectra of **1** recorded at 170 and 393 K corresponding to LS to HS states, respectively.

The modes that mostly contribute to the corresponding peaks are being labeled with the corresponding irreducible representation of the D_{2d} point group symmetry. An artificial Lorentzian broadening of 5 cm^{-1} was used. The intensities are normalized to the highest intensity for each spin state.

The Raman spectra are dominated by the bands related to the pyridine vibration. In the range of 1000–1100 cm^{-1} , they show stronger diagnostic features for monitoring the crossover from

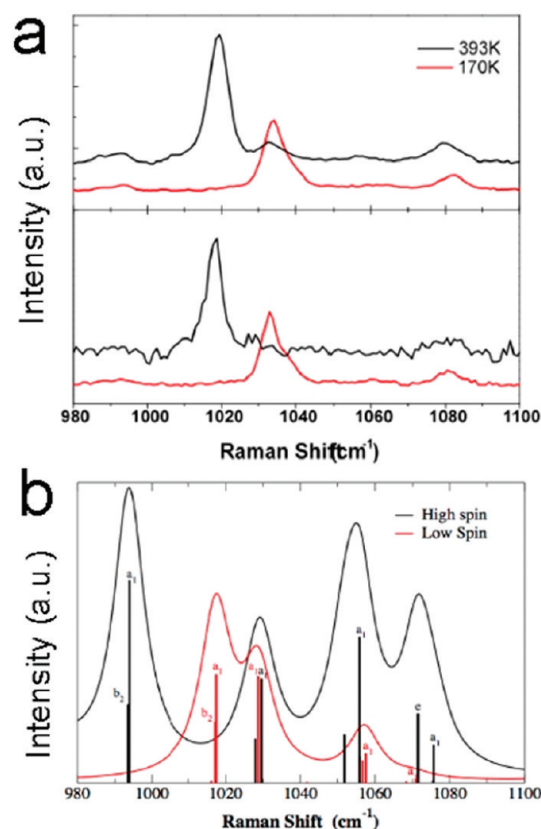


Figure 5. (a) Raman spectra of the bulk (top curve) and a thin deposit (bottom curve) recorded at 170 K (LS – red curve) and 393 K (HS – black curve). (b) Calculated Raman spectra for the $[\text{Fe}(\text{bpp})_2]^{2+}$ core for both high (black) and low (red) Spin.

LS to HS states. For both the pristine powder sample and the thin film, the maximum in the most intense peak shifts from about 1034 cm^{-1} for the LS state to 1019 cm^{-1} for the HS state. microRaman experiments show that **1** retains its SCO nature when the solvent shrinks slowly; conversely, when fast shrinkage is employed, the thin deposit loses the spin transition.

Theoretical calculations of Raman spectra for the $[\text{Fe}(\text{bis}(\text{pyrazolyl})\text{pyridine})_2]^{2+}$ core were performed within the TURBOMOLE quantum chemistry package.⁵⁰ The density functional theory (DFT) level of theory with the BP86 exchange correlation functional^{51,52} along with a basis of triple- ζ quality (def2-TZVP)⁵³ was used. D_{2d} symmetry was retained in the molecule.

The b_2 and a_2 breathing modes involving pyridine rings were found at 994 cm^{-1} (experimental 1019 cm^{-1}) for the HS state and at 1017 cm^{-1} (experimental 1034 cm^{-1}) for the LS state (Figure 5b). These modes are, more specifically, stretching/squeezing the $\text{Fe}(\text{II})\text{--N}$ (in the pyridine ring) bond, pointing to the fact that these are similar vibrational modes for two different (spin) states of the molecule. The shift toward lower frequencies of about 20 cm^{-1} when going from the LS to HS spin state can be understood by increasing the $\text{Fe}(\text{II})\text{--N}$ bond length upon the spin transition ($\sim 10\%$ increase), consequently decreasing the bond strength. Peaks for both HS and LS at $\sim 1030\text{ cm}^{-1}$ belong to an a_1 irreducible representation and involving skeletal movement, but a clear connection involving the $\text{Fe}(\text{II})\text{--N}$ bond is missing. This mode is clearly observed experimentally at 1032 cm^{-1} in the HS state, whereas in the LS state it overlaps the a_1 and b_1 pyridine ring breathing modes. Higher frequencies were mostly

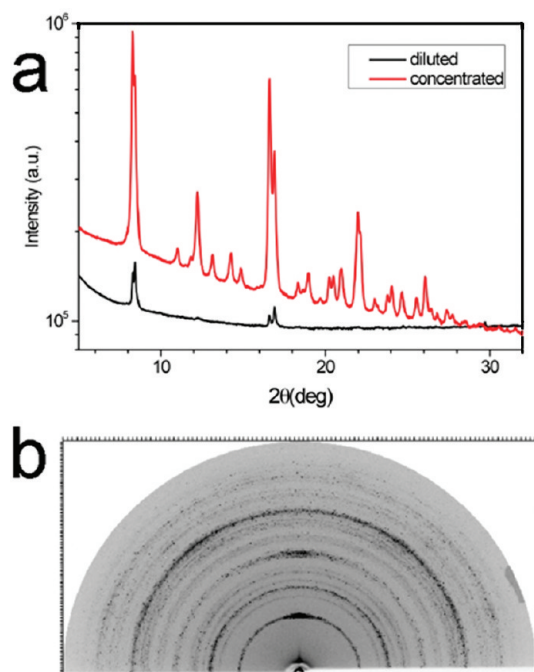


Figure 6. (a) XRD patterns of thin deposits of **1** obtained by drop casting diluted (black curve) and concentrated (red curve) solutions. (b) Two-dimensional GID image of the concentrated film recorded by using synchrotron radiation ($\lambda = 1.5498 \text{ \AA}$, angle of incidence = 1°).

H-bond-vibration-dominant. None of these vibrations are predicted to show a dramatic shift upon spin transition. The shift of the breathing mode of the pyridine groups in the HS/LS transition has also been observed in the $[\text{Fe}(\text{pmea})(\text{NCS})_2]$ parent compound.⁴⁹ Figure 5b shows the calculated Raman spectra for the $[\text{Fe}(\text{bpp})_2]^{2+}$ core for both HS and LS states.

Thin deposits on silicon substrates were found to be polycrystalline and, regardless of the concentration of the starting solution, exhibit the same crystalline structure, as shown by the coincidence of the position of the strongest Bragg peaks of the XRD patterns (Figure 6a). The presence of few reflections in the diffractogram of the diluted film indicates that it consists of crystallites preferentially oriented with the substrate surface. However, for the film obtained from a more concentrated solution, hkl reflections are recorded in the diffraction patterns, and the 2D-GID image (Figure 6b) shows that both Debye rings having a homogeneous intensity distribution and (00 L) rings undergo an intensity enhancement along the central part of the detector. This indicates that randomly oriented crystallites coexist with a minority of crystallites, likely lying close to the surface substrate and having a preferential orientation with respect to the substrate. The structural investigation of a typical patterned thin film indicates that inside the patterned region probed by the X-ray beam ($23 \times 0.5 \text{ mm}^2$) the molecules that assemble (organize) in crystalline domains are able to produce strong diffraction peaks.

CONCLUSIONS

We have presented thin deposits and patterning of room-temperature-switchable 1-D spin-crossover compounds on a surface into stripes made by randomly oriented crystallites. We showed how the compound can be lithographically processed into crystalline micrometric and submicrometric structures on a

technologically relevant surface preserving the functional properties of switching. The lithographic process provides ordered structures; furthermore, it accelerates the timing of crystal formation from a day to less than 1 h.

The successful patterning of crystalline aggregates of a representative complex, with controlled size at the micrometric (and thus optically accessible) frontier, can easily be scaled down to smaller (nanometric) length scales. Furthermore, the approach that is used can be extended to many other spin-crossover compounds. In this respect, our work represents a relevant breakthrough in view of the technological application of this class of materials in the direction of a new generation of sensing devices and molecular memories.

AUTHOR INFORMATION

Corresponding Author

*E-mail: m.cavallini@bo.ismn.cnr.it.

ACKNOWLEDGMENT

We thank Emanuela Margapoti, Fabio Biscarini, Pablo Stoliar, Annalisa Calò, and Mirko Prezioso for their help and suggestions. This work was partially supported by projects ESF-SONS2-FUNSMARTS II and ESF-EURYI DYMOT.

REFERENCES

- (1) Bonhommeau, S.; Guillon, T.; Daku, L. M. L.; Demont, P.; Costa, J. S.; Letard, J. F.; Molnar, G.; Bousseksou, A. *Angew. Chem., Int. Ed.* **2006**, *45*, 1625.
- (2) Bousseksou, A.; Molnar, G.; Demont, P.; Menegotto, J. *J. Mater. Chem.* **2003**, *13*, 2069.
- (3) Letard, J. F.; Guionneau, P.; Goux-Capes, L. Towards Spin Crossover Applications. In *Spin Crossover in Transition Metal Compounds III*; Gülich, P., Goodwin, H. A., Eds.; Topics in Current Chemistry; Springer: Berlin, 2004; Vol. 233; p 221.
- (4) Kahn, O.; Krober, J.; Jay, C. *Adv. Mater.* **1992**, *4*, 718.
- (5) Kahn, O.; Martinez, C. *J. Science* **1998**, 279, 44.
- (6) Cavallini, M.; Bergenti, I.; Milita, S.; Ruani, G.; Salitros, I.; Qu, Z. R.; Chandrasekar, R.; Ruben, M. *Angew. Chem., Int. Ed.* **2008**, *47*, 8596.
- (7) (a) Cavallini, M.; Facchini, M.; Albonetti, C.; Biscarini, F. *Phys. Chem. Chem. Phys.* **2008**, *10*, 784. (b) Cavallini, M.; Gomez-Segura, J.; Albonetti, C.; Ruiz-Molina, D.; Veciana, J.; Biscarini, F. *J. Phys. Chem. B* **2006**, *110*, 11607.
- (8) Breuning, E.; Ruben, M.; Lehn, J. M.; Renz, F.; Garcia, Y.; Ksenofontov, V.; Gutlich, P.; Wegelius, E.; Rissanen, K. *Angew. Chem., Int. Ed.* **2000**, *39*, 2504.
- (9) Gutlich, P.; Garcia, Y.; Goodwin, H. A. *Chem. Soc. Rev.* **2000**, 29, 419.
- (10) Sato, O. *Acc. Chem. Res.* **2003**, *36*, 692.
- (11) Bonhommeau, S.; Guillon, T.; Daku, L. M. L.; Demont, P.; Costa, J. S.; Letard, J. F.; Molnar, G.; Bousseksou, A. *Angew. Chem., Int. Ed.* **2006**, *45*, 1625.
- (12) Varret, F.; Boukheddaden, K.; Codjovi, E.; Goujon, A. *Hyperfine Interact.* **2005**, *165*, 37.
- (13) Varret, F.; Boukheddaden, K.; Codjovi, E.; Maurin, I.; Tokoro, H.; Ohkoshi, S.; Hashimoto, K. *Polyhedron* **2005**, *24*, 2857.
- (14) Ross, T. M.; Neville, S. M.; Innes, D. S.; Turner, D. R.; B., M.; Murray, K. S. *Dalton Trans.* **2010**, 39, 149.
- (15) Boca, R.; Renz, F.; Boca, M.; Fuess, H.; Haase, W.; Kickelbick, G.; Linert, W.; Vrbova-Schikora, M. *Inorg. Chem. Commun.* **2005**, *8*, 227.
- (16) Niel, V.; Martinez-Agudo, J. M.; Munoz, M. C.; Gaspar, A. B.; Real, J. A. *Inorg. Chem.* **2001**, *40*, 3838.

- (17) Holland, J. M.; McAllister, J. A.; Lu, Z. B.; Kilner, C. A.; Thornton-Pett, M.; Halcrow, M. A. *Chem. Commun.* **2001**, 577.
- (18) Bonhommeau, S.; Molnar, G.; Galet, A.; Zwick, A.; Real, J. A.; McGarvey, J. J.; Bousseksou, A. *Angew. Chem., Int. Ed.* **2005**, *44*, 4069.
- (19) Larionova, J.; Salmon, L.; Guarl, Y.; Tokarev, A.; Molvinger, K.; Molnar, G.; Bousseksou, A. *Angew. Chem., Int. Ed.* **2008**, *47*, 8236.
- (20) Coronado, E.; Galan-Mascaros, J. R.; Monrabal-Capilla, M.; Garcia-Martinez, J.; Pardo-Ibanez, P. *Adv. Mater.* **2007**, *19*, 1359.
- (21) Forestier, T.; Mornet, S.; Daro, N.; Nishihara, T.; Mouri, S.; Tanaka, K.; Fouche, O.; Freysz, E.; Letard, J. F. *Chem. Commun.* **2008**, 4327.
- (22) Gutlich, P.; Hauser, A.; Spiering, H. *Angew. Chem., Int. Ed.* **1994**, *33*, 2024.
- (23) Cambi, L.; Cagnasso, A. *Atti. Accad. Naz. Lincei, Cl. Sci. Fis., Mat. Nat., Rend.* **1931**, *13*, 809.
- (24) Cambi, L.; Szego, L. *Ber. Dtsch. Chem. Ges. B* **1931**, *64*, 259.
- (25) Armand, F.; Badoux, C.; Bonville, P.; Ruaudelteilxier, A.; Kahn, O. *Langmuir* **1995**, *11*, 3467.
- (26) Soyer, H.; Dupart, E.; Gomez-Garcia, C. J.; Mingotaud, C.; Delhaes, P. *Adv. Mater.* **1999**, *11*, 382.
- (27) Soyer, H.; Mingotaud, C.; Boillot, M. L.; Delhaes, P. *Langmuir* **1998**, *14*, 5890.
- (28) Cobo, S.; Molnar, G.; Real, J. A.; Bousseksou, A. *Angew. Chem., Int. Ed.* **2006**, *45*, 5786.
- (29) Molnar, G.; Cobo, S.; Real, J. A.; Carcenac, F.; Daran, E.; Vien, C.; Bousseksou, A. *Adv. Mater.* **2007**, *19*, 2163.
- (30) Bousseksou, A.; Molnar, G.; Demont, P.; Menegotto, J. J. *Mater. Chem.* **2003**, *13*, 2069.
- (31) Agusti, G.; Cobo, S.; Gaspar, A. B.; Molnar, G.; Moussa, N. O.; Szilagyi, P. A.; Palfi, V.; Vieu, C.; Munoz, M. C.; Real, J. A.; Bousseksou, A. *Chem. Mater.* **2008**, *20*, 6721.
- (32) Cavallini, M. *J. Mater. Chem.* **2009**, *19*, 6085.
- (33) (a) Cavallini, M.; Albonetti, C.; Biscarini, F. *Adv. Mater.* **2009**, *21*, 1043. (b) Greco, P.; Cavallini, M.; Stoliar, P.; Quiroga, S. D.; Dutta, S.; Zachini, S.; Lapalucci, M. C.; Morandi, V.; Milita, S.; Merli, P. G.; Biscarini, F. *J. Am. Chem. Soc.* **2008**, *130*, 1177. (c) Serban, D. A.; Greco, P.; Melinte, S.; Vlad, S.; Dutu, C. A.; Zacchini, S.; Iapalucci, M. C.; Biscarini, F. *M. C. Small* **2009**, *5*, 1117.
- (34) Thibault, C.; Molnar, G.; Salmon, L.; Bousseksou, A.; Vieu, C. *Langmuir* **2010**, *26*, 1557.
- (35) Rajadurai, C.; Schramm, F.; Brink, S.; Fuhr, O.; Ghafari, M.; Kruk, R.; Ruben, M. *Inorg. Chem.* **2006**, *45*, 10019.
- (36) (a) Cavallini, M.; Murgia, M.; Biscarini, F. *Nano Lett.* **2001**, *1*, 193. (b) Cavallini, M.; Simeone, F. C.; Borgatti, F.; Albonetti, C.; Morandi, V.; Sangregorio, C.; Innocenti, C.; Pineider, F.; Annese, E.; Panaccione, G.; Pasquali, L. *Nanoscale* **2010**, *2*, 2069–2072.
- (37) (a) Cavallini, M.; Stoliar, P.; Moulin, J. F.; Surin, M.; Leclere, P.; Lazzaroni, R.; Breiby, D. W.; Andreasen, J. W.; Nielsen, M. M.; Sonar, P.; Grimsdale, A. C.; Mullen, K.; Biscarini, F. *Nano Lett.* **2005**, *5*, 2422. (b) Corradini, V.; Menozzi, C.; Cavallini, M.; Biscarini, F.; Betti, M. G.; Mariani, C. *Surf. Sci.* **2003**, *532*, 249. (c) Menozzi, C.; Corradini, V.; Cavallini, M.; Biscarini, F.; Betti, M. G.; Mariani, C. *Thin Solid Films* **2003**, *428*, 227.
- (38) (a) Cavallini, M.; Facchini, M.; Massi, M.; Biscarini, F. *Synth. Met.* **2004**, *146*, 283. (b) Leyva, A. G.; Stoliar, P.; Rosenbusch, M.; Lorenzo, V.; Levy, P.; Albonetti, C.; Cavallini, M.; Biscarini, F.; Troiani, H. E.; Curiale, J.; Sanchez, R. D. *J. Solid State Chem.* **2004**, *177*, 3949.
- (39) Cavallini, M.; Biscarini, F. *Nano Lett.* **2003**, *3*, 1269.
- (40) Monahan, J.; Gewirth, A. A.; Nuzzo, R. G. *Anal. Chem.* **2001**, *73*, 3193.
- (41) Cavallini, M.; Biscarini, F.; Gomez-Segura, J.; Ruiz, D.; Veciana, J. *Nano Lett.* **2003**, *3*, 1527.
- (42) Martinez-Otero, A.; Evangelio, E.; Alibes, R.; Bourdelande, J. L.; Ruiz-Molina, D.; Busque, F.; Hernando, J. *Langmuir* **2008**, *24*, 2963.
- (43) Bystrenova, E.; Facchini, M.; Cavallini, M.; Cacace, M. G.; Biscarini, F. *Angew. Chem., Int. Ed.* **2006**, *45*, 4779.
- (44) (a) Cavallini, M.; Aloisi, G.; Bracali, M.; Guidelli, R. *J. Electroanal. Chem.* **1998**, *444*, 75. (b) Cavallini, M.; Bracali, M.; Aloisi, G.; Guidelli, R. *Langmuir* **1999**, *15*, 3003.
- (45) Coronado, E.; Marti-Gastaldo, C.; Galan-Mascaros, J. R.; Cavallini, M. *J. Am. Chem. Soc.* **2010**, *132*, 5456.
- (46) Leclere, P.; Surin, M.; Lazzaroni, R.; Kilbinger, A. F. M.; Henze, O.; Jonkheijm, P.; Biscarini, F.; Cavallini, M.; Feast, W. J.; Meijer, E. W.; Schenning, A. *J. Mater. Chem.* **2004**, *14*, 1959.
- (47) Deegan, R. D.; Bakajin, O.; Dupont, T. F.; Huber, G.; Nagel, S. R.; Witten, T. A. *Nature* **1997**, *389*, 827.
- (48) Melucci, M.; Barbarella, G.; Zambianchi, M.; Benzi, M.; Biscarini, F.; Cavallini, M.; Bongini, A.; Fabbri, S.; Mazzeo, M.; Anni, M.; Gigli, G. *Macromolecules* **2004**, *37*, 5692.
- (49) Brehm, G.; Reiher, M.; Le Guennic, B.; Leibold, M.; Schindler, S.; Heinemann, F. W.; Schneider, S. *J. Raman Spectrosc.* **2006**, *37*, 108.
- (50) Ahlrichs, R.; Bar, M.; Haser, M.; Horn, H.; Kolmel, C. *Chem. Phys. Lett.* **1989**, *162*, 165.
- (51) Perdew, J. P. *Phys. Rev. B* **1986**, *33*, 8822.
- (52) Becke, A. D. *Phys. Rev. A* **1988**, *38*, 3098.
- (53) Weigend, F.; Ahlrichs, R. *Phys. Chem. Chem. Phys.* **2005**, *7*, 3297.